Comparison of BCF-10, BCF-12, and BCF-20 Scintillating Fibers for Use in a 1-Dimensional Linear Sensor

David L. Chichester, *Senior Member, IEEE*, Scott M. Watson, and James T. Johnson

***Abstract*—One-dimensional fiber-bundle arrays may prove useful in a number of radiation sensing applications where radiation detection over large areas is needed. Tests have been performed to evaluate the light generation and transmission characteristics of 15-meter long, 10-fiber bundles of BCF-10, BCF-12, and BCF-20 scintillating fibers (Saint Gobain) exposed to collimated gamma-ray sources. The test set-up used one R9800 (Hamamatsu) photomultiplier tube (PMT) at each end, with a high-speed waveform digitizer to collect data. Time constraints were imposed on the waveform data to perform time-of-flight analysis of the events in the fiber bundles, eliminating spurious noise pulses in the high gain PMTs and also allowing 1-dimensional localization of interactions along the lengths of the fiber bundles. Measurements show that the spatial response of these three fibers is linear over at least 15-m lengths and that, with the equipment used here, the spatial resolution for events irradiating 1 cm of fiber (using a collimated source) ranges from 50 cm to 60 cm over the entire length of the bundles. The efficiency for detecting events varies along the length of the arrays, with the sensitivity at the midpoint (half of the distance) of an array ranging from ∼2X to ∼3X the efficiency at the ends, depending on the length of the fiber-bundle array and the self-absorption factor for each fiber's scintillation light. Compared to prior work, a 20-fold improvement in detection sensitivity has been shown for this technique, most likely due to improved optical coupling and improved signal analysis.**

***Index Terms*—Fiber optics, radiation detectors, radiation monitoring, time-domain analysis.**

I. Introduction

LONG, small-diameter, organic scintillating fiber bundle (SFB) assemblies are under investigation at Idaho National Laboratory (INL), applied as one-dimensional (1-D) linear sensors to monitor and characterize ionizing radiation fields over long distances or over large areas. Due to the low-Z value of the polystyrene used to make these fibers, the primary mechanism for radiation detection in these detectors is Compton scattering, where Compton-scattered electrons deposit energy in the fibers leading to visible-light generation. This light is detected and measured using photomultipliers attached to each end of the fiber bundles.

There are several arenas that need simple, distributed sensor networks to monitor radiation fields, including radiation health physics, system monitoring at large facilities (nuclear reactors, nuclear material processing facilities, high-energy particle accelerators, hospitals, etc.), and nuclear security and nonproliferation. Traditionally, discrete instrumentation is placed at closely-spaced intervals, whereas continuous sensors can eliminate gaps or weak spots between such sensor modules, and at the same time reduce requirements for support infrastructure including installed equipment and its mounting and power consumption. This paper presents an overview of prior research in this area and then presents the results of recent studies performed to characterize three different candidate SFB materials. This effort builds upon prior work in the field by providing the first comparison of position linearity and position resolution for all three types of fibers. Using the same PMT and data acquisition electronics, the paper also gives a head-to-head comparison of detection efficiency for all three types of fibers.

II. Background Information

Early SFB assemblies for radiation detection and measurement used thousands of short length (∼10 cm long) scintillating fibers, such as NE-103, bundled together to create a single sensor unit, usually a right cylinder incorporating plastic fibers embedded in a plastic matrix [1], [2]. This form factor, originally developed for space research, provided a directionally sensitive neutron probe and was subsequently improved and applied to terrestrial survey. Other researchers subsequently developed several other scintillating fiber detectors for measuring neutrons in the same cylindrical form factor [3]–[8]. Over time, detector developers eventually began to use boron- or lithium-based fibers to increase the thermal neutron sensitivity of their instruments.

As longer-length-fiber scintillating fibers became available, their use in radiation instrumentation grew along two different paths. In the first case, researchers used newly available long-length fibers to create neutron and gamma-ray detectors using large-area ribbons, or "sheets" of fibers, to make flexible ribbon detectors or large-area detector panels [9], [10]. In one case, over 250 km of ∼2-m-long glass fibers were used to create a 5 m^2 sensor panel [11]. Large-area radiation instrumentation based on scintillating fibers found particular traction within the

Manuscript received November 11, 2012; revised January 20, 2013; accepted July 23, 2013. Date of publication September 17, 2013; date of current version October 09, 2013. This work was supported by Idaho National Laboratory's Laboratory for Directed Research and Development (LDRD) program. Idaho National Laboratory is operated for the U.S. Department of Energy by Battelle Energy Alliance under DOE contract DE-AC07-05-ID14517.

The authors are with Idaho National Laboratory, Idaho Falls, ID 83415 USA (e-mail: david.chichester@inl.gov; scott.watson@inl.gov; james.johnson@inl.gov).

Color versions of one or more of the figures in this paper are available online at http://ieeexplore.ieee.org.

Digital Object Identifier 10.1109/TNS.2013.2277799

TABLE I
IMPORTANT PARAMETERS FOR BCF-10, BCF-12, AND BCF-20 [26]

Parameter	BCF-10	BCF-12	BCF-20
Core material	Polystyrene (common for all three)		
Core refractive index	1.60 (common for all three)		
Density	1.05 (common for all three)		
Emission peak, nm	432	435	492
Decay time, ns	2.7	3.2	2.7
1/e length, m*	2.2	2.7	>3.5
# of photons per MeV**	~8000	~8000	~8000

* *For 1-mm diameter fiber; measured with a bialkali cathode photomultiplier tube(PMT).*
** *For minimum ionizing particle (MIP), corrected for PMT sensitivity.*

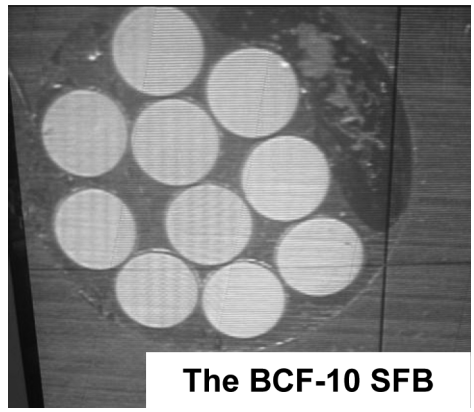

Fig. 1. A magnified in-process quality control photo of one end of the BFC-10 bundle, showing fiber location and polish within the end fitting. Note the epoxy void in the upper right. This does not affect operation because all of the fibers are uniformly held by the epoxy potting. For scale, note that the fibers are 1 mm in diameter.

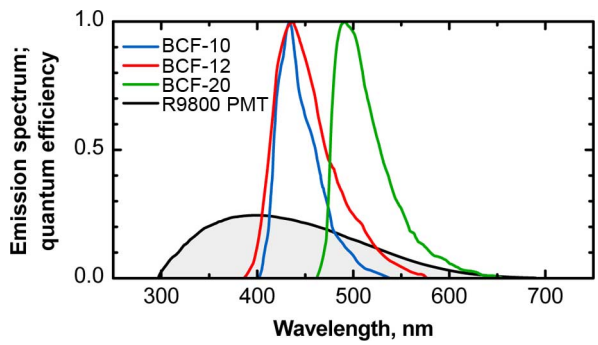

Fig. 2. The emission spectra for BCF-10, BCF-12, and BCF-20, together with the energy-dependent quantum efficiency for the R9800 PMT [26].

community of physicists developing instruments for high-energy particle accelerator facilities [12]–[14]. Scintillating fibers have also found application in health physics and nuclear nonproliferation [15], [16].

In the second implementation, the flexible, long-length scintillating fibers were configured to form line detectors. In some cases, short lengths of scintillating fiber the order of one cm in length were spliced together with non-scintillating fibers so the scintillating portions served as point detectors. This configuration was applied in medical physics and radiation oncology, when thin fibers are inserted into patients intravenously to measure the dose applied during radiation therapy [17]–[20]. Thin continuous fibers have also been used as area photon radiation monitors for health physics protection in accelerator beam halls and at nuclear reactors [21]–[25]. In particular, recent research described by Nohtomi *et al.* provides a valuable starting point for considering the use of SFB detectors for nuclear security and nonproliferation [25].

III. EQUIPMENT AND METHODS

Four fiber bundles, each containing ten fibers, were assembled for this project by Saint Gobain Crystals (Hiram, Ohio, USA) using their commercial scintillating fibers BCF-10, BCF-12, and BCF-20 [26]. The vendor's technical specifications for these materials are presented in Table I. BCF-10 fibers were used to make one 2.2-m-long bundle and one 14.85-m-long bundle. The bundle with BCF-12 was 15.18-m long and the BCF-20 bundle was 15.28-m long. The fibers within each bundle were loosely bunched together and packaged within a light-tight, flexible vinyl tubing. The approximate outside diameters of these bundles is 0.5 cm. The ends of the bundles were potted into a larger diameter (1-cm) end fitting using transparent epoxy. The fibers were cut off flat in a near-polished condition by the vendor; a photograph of the potted fibers at one end of one of the bundles is shown in Fig. 1. As a test to determine if further polishing would be beneficial, the ends of the 2.2-m fiber were finished with at our facilities with a graded-approach, hand-sanding technique using 600-grit, 800-grit, and 1000-grit wet sand, and then a 1200-grit diamond wheel. After this, the ends of the SFBs were hand polished using a felt polishing wheel with iron-oxide slurry. Minimal improvement was observed.

TABLE II
IMPORTANT PARAMETERS FOR THE R9800 PMT [27]

Parameter	R9800 PMT
Rise time, ns	1.0
Transit time spread (full-width half maximum, FWHM), ns	0.270
Wavelength of maximum response, nm	420
Gain	1.1×10^6
Photocathode material	Bialkali
Window material	Borosilicate glass
Window effective diameter, cm	2.2

The specially-made end fittings were designed to allow them to be easily attached or detached from a pair of Hamamatsu R9800 photomultiplier tubes (PMTs) built as Hamamatsu H10580 PMT assemblies with matching end fixtures. Technical specifications for the R9800 PMT, as provided by the vendor, are provided in Table II. A comparison of the emission spectra

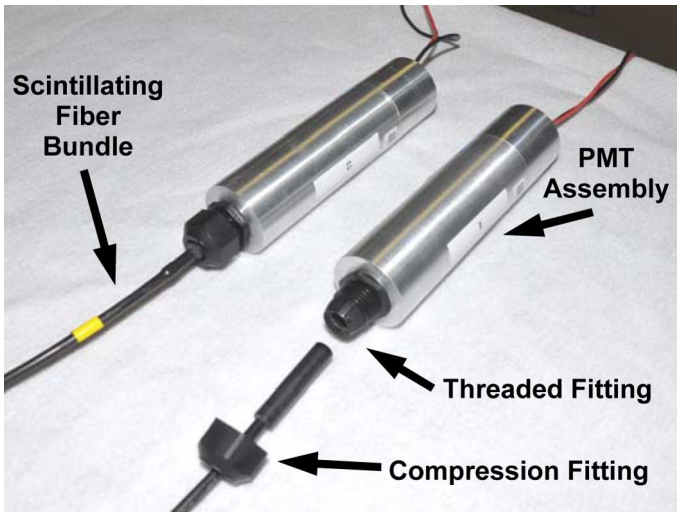

Fig. 3. A photograph of two PMT assemblies. The assembly on the left has been connected to a SFB; the assembly on the right is staged for assembly.

for the three types of fibers, and the R9800 PMT quantum efficiency spectrum are shown together in Fig. 2 [26], [27].

As mentioned, the PMTs are housed within light-tight aluminum cases; a threaded plastic fixture screws into the aluminum case and provides a swage-like compression fitting to capture the ferrule on the end of the bundle, stabilize it, and hold it against the cathode of the spring-loaded PMT. Each PMT assembly includes a replaceable transparent optical silicone pad for index matching between the bundle and the PMT. A photograph of the PMT assembly, showing attachment of an SFB, is presented in Fig. 3.

Measurements were performed by digitizing the output signals of the PMT's using two channels of an Acquiris DC282 10-bit high-speed digitizer (4 Gs/s). The DC282 was controlled by National Instruments LabView software. An application specific virtual instrument (VI) was developed using LabView that allowed the difference in arrival time of the signals between the two PMT's to be recorded, triggering off of either PMT. For this implementation, one of the two PMTs was used as a hard-wired trigger with the Acquiris digitizer board. Sufficient pre-trigger waveforms were saved so that, for each hardware trigger event, analysis could be performed to identity leading pulses or following pulses in the other PMT. The existence of coincident pulses in the other PMT was determined using the VI software. Typical noise levels from each PMT were on the order of 5 mV; trigger levels for both the hardware trigger and the software pulse-discriminator setting were typically set at 10 mV.

Tests were performed to 'gain-match' the two PMTs but this process was not perfect. Because of this, the absolute efficiency of the system was not perfect along the entire length; when an event occurs closer to one PMT than the other the signal arriving at the further PMT is reduced in magnitude due to attenuation. The imperfect gain-matching in these cases resulted in one side of the fiber having a higher absolute efficiency than the other, since the trigger values were nearly identical for both PMTs. The does not present a problem for the technique, however, because it is possible to measure the position dependent efficiency of the fiber (using a collimated source scanned along the length of the bundle) to develop a linear efficiency correction factor for the length of the fiber. Slight timing errors occurred due to latency between the hardware and software derived triggers for each PMT input to the digitizer but these were $<1\%$ of the measured signal time differences; this was determined using an electronic pulser injected into the data acquisition system and through studying the PMT performance with the PMTs next to each other using a light source.

Prior to performing the experiments described below, the PMT's were optimized and gain matched. This was done using the 2-m BCF-10 fiber with a collimated ^{60}Co check source located in the middle of the SFB. (The collimation was achieved by using lead bricks to create a slit collimator. The check source was recessed approximately 5 cm below the edge of the slit, which was 1 cm wide. The same collimation set-up, exposing 1 cm of fiber, was used for all cases in this paper where collimation was used.) The signal amplitudes from the two PMTs were monitored and the high voltage (HV) setting for each PMT was adjusted until both units had approximately the same output amplitude. The same procedure was implemented for the other SFBs as a system check but no further HV adjustments were necessary.

The experiments involved placing a gamma-ray check source, either an uncollimated ^{60}Co disk source producing 3.8 mrem hr^{-1} (38 μSv hr^{-1}) on contact with the fiber (data collected for 1800 s) or a collimated ^{137}Cs disk source producing 14 mrem hr^{-1} (140 μSv hr^{-1}) on contact with the fiber (data collected for 900 s) adjacent to the SFBs at different locations. The position of 0 meters corresponded to the front face of one of the PMTs (PMT1). Time-difference measurements between the PMTs, made using the digitizer, were determined according to the equation $\Delta t = t_{PMT2} - t_{PMT1}$ such that a pulse occurring closer to PMT1 (closer to position 0 m) would register before the pulse reached PMT2. Because of this, pulses in the half of the SFB closer to PMT1 (0 m) would register with a positive time difference while those occurring in the other half of the SFB (closer to PMT2) registered as negative time differences. Pulses occurring close to the center of a SFB occurred near a time difference of zero.

IV. Experiments Analyzing SFB Performance

The performance of a bundle operating as a linear detector can be characterized by its coincident pulse height amplitude (and attenuation versus path length), position linearity, position resolution, efficiency, and linearity versus rate. Measurements for each of these characteristics are presented in the following subsections.

A. Coincident Pulse Height Amplitude

A plot showing a pulse-height histogram for the voltage signals from PMT2 using BCF-20 is presented in Fig. 4. This data corresponds only to signals measured in coincidence with a signal in PMT1, data is shown for the ^{60}Co source at 1, 3, 5, 7, 9, 11, and 13 m along the bundle. A discriminator level of 10 mV was used for noise rejection in the system, triggering was performed using leading edge triggers on each waveform. The most intense measurement case corresponds to having the source at the center of the SFB. With a long 1/e absorption length, BCF-20

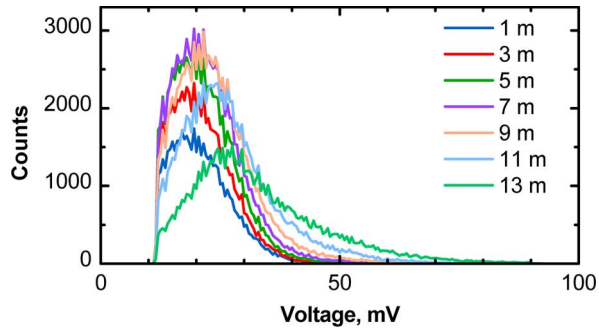

Fig. 4. Plot of the average pulse-height histogram for waveforms from PMT2, when a coincident pulse is measured in PMT1, for BCF-20 over an 1800 s period using a ^{60}Co source at 1, 3, 5, 7, 9, 11, and 13 m.

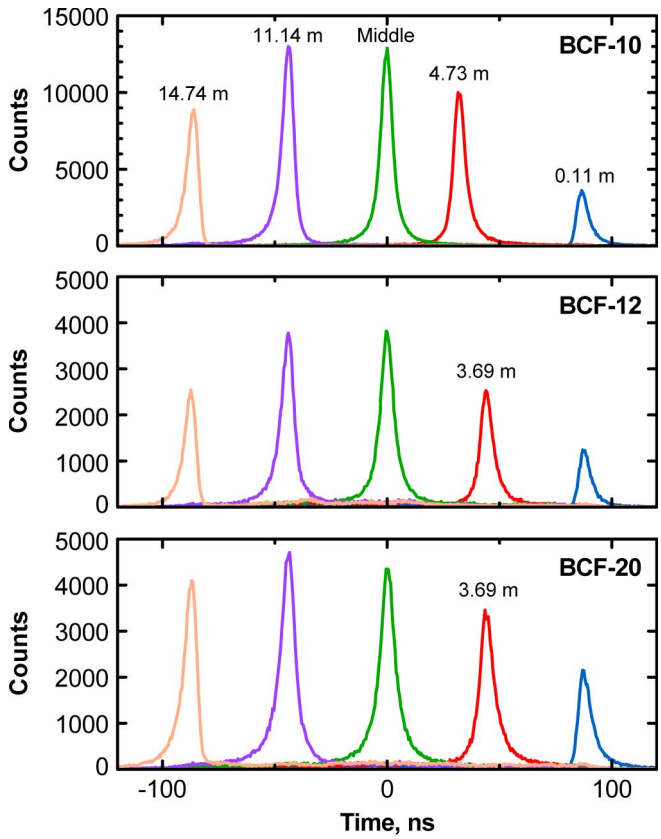

Fig. 5. These three plots show the timing resolution for measuring events in each SFB using a well-collimated ^{137}Cs source. (Note: For the BCF-12 and BCF-20 SFBs, the second measurements taken from zero (nominal 4.73 m for BCF-10, red trace) were taken at 3.69 m).

showed the best signal-to-noise transmission towards the ends of the SFB.

B. Position Linearity

Using the collimated ^{137}Cs source, multiple measurements of signal-time differences were recorded for 900 s using the three SFBs at five different locations along the length of each SFB. For BCF-10 these locations were 0.11, 4.73, 7.42 (the middle), 11.14, and 14.74 m. For BCF-12 and BCF-20, the second measurement position was 3.69 m instead of 4.73 m and the 7.42 m location was replaced with the middle of that fiber. Plots of

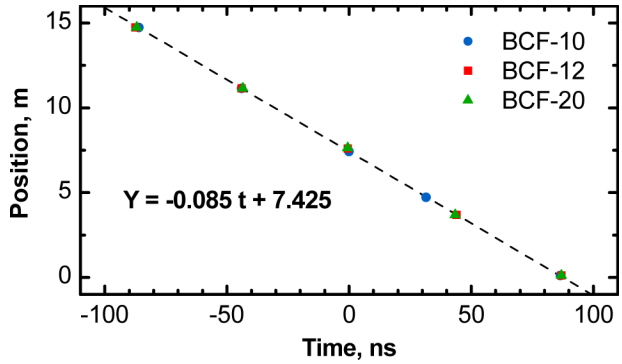

Fig. 6. Plot showing the relationship between time and position for BCF-10, BCF-12, and BCF-20. (The nonlinear component to this fit is $< 10^{-5}$).

TABLE III
TEMPORAL AND SPATIAL RESOLUTION OF THE BCF-10, BCF-12, AND BCF-20 SCINTILLATING FIBER BUNDLES.[26]

Resolving time (FWHM), ns (± 0.5 ns)					
SFB	**0.11 m**	**3.82 m**	**7.64 m**	**11.46 m**	**15.17 m**
BCF-10	6.1	6.2	6.3	6.2	6.2
BCF-12	6.0	6.7	6.9	6.7	6.1
BCF-20	6.2	7.5	7.8	7.5	6.6
Spatial resolution (FWHM), cm (± 4.2 cm)					
SFB	**0.11 m**	**3.82 m**	**7.64 m**	**11.46 m**	**15.17 m**
BCF-10	51.7	52.6	53.4	52.6	52.6
BCF-12	50.9	56.8	58.5	56.8	51.7
BCF-20	52.6	63.6	66.1	63.6	56.0

the time difference for signals measured during these 15 measurements are presented in Fig. 5. The relationship between locations along the SFB and signal time differences is clearly illustrated in these plots. The centroid position for each measurement has been plotted versus time difference in Fig. 6; the relationship is linear over the ∼15-m length of these three SFBs. For this setup the relationship between position and time yields conversion relations (speed of light in the fibers) of 17.0 ± 1.6 cm ns^{-1} for BCF-10, 16.8 ± 1.6 cm ns^{-1} for BCF-12, and 17.0 ± 1.6 cm ns^{-1} for BCF-20. This should be compared with the ideal speed of light in these plastics, determined using the index of refraction $n = 1.60$ from Table I and the equation $v = c/n$, of $v = 18.8$ cm ns^{-1}. The difference between experiment and theory stem from several factors including delays in the PMT and preamplifier responses. Scattering and reflection as the light transits down the length of the SFB also plays a role [28].

C. Position Resolution

The spatial resolution for these measurements is extracted from full-width half-maximum of the time differences for the individual measurements seen in Fig. 5. This information is presented in Table III.

These time differences have been converted to distance, using the conversion factor of 8.5 cm ns^{-1} from Fig. 6. Overall

the spatial resolution across the 15-m long SFBs is between 50–60 cm. The spatial resolution is slightly better towards the ends than in the middle, most likely due to the reduced effect light scattering has on the signal reaching the nearer PMT versus the farther PMT. This can be seen in the plots of Fig. 5 where the time plots near the ends of the SFBs becomes more asymmetric, with the inner edges of these distributions (the side of the distribution closer to the middle of the SFBs) looking more like 'pure' Gaussian distributions. When an event starts near to one of the PMTs it undergoes less light scattering along that journey than corresponding photons headed towards the other PMT. This reduced scattering, in conjunction with the fact that photons reaching the other end are reduced in intensity and closer to the trigger threshold for these 15-m fibers, lead to this asymmetry in position determination. (An explanation of these phenomena using modeling is presented in [29].) The absolute signal intensity from the BCF-10 SFB was significantly larger than for the other two (next section.) This leads to a better signal-to-noise characteristic for these SFBs, which is likely the reason why the spatial resolution for BCF-10 is the best of the three.

D. Efficiency

The measurement efficiency for the three SFBs was determined from the 15 measurements of Fig. 5 using the collimated ^{137}Cs; this information is presented in Fig. 7. The SFBs are most sensitive in their middles, where the signal-to-noise characteristics in the PMTs are balanced. As the source is moved towards the ends it becomes more likely that, for any particular event, the signal reaching the far PMT will either be too noisy (failing the pulse-shape analysis in the LabView VI algorithm) or too weak (falling below the trigger level of the count discriminator). Since the signals as measured by the far PMTs are weak the observed end-to-end variation is a result of the small differences in the gain/trigger settings between to the PMTs rather than some sort of inherent differences in absolute efficiency of the ends of the fibers. To confirm this, tests were performed by switching the fibers around (plugging the ends into opposite PMTs) and repeating a set of these tests. These results remained the same. This demonstrates the important of performing a relative calibration of a system along its length if quantitative radiation field measurements are needed.

As presented above, the BCF-10 SFB is the most sensitive of the three tested when coupled with this PMT, having a maximum efficiency of 26.9 counts s^{-1} per mrem hr^{-1} (2.69 counts s^{-1} per μSv hr^{-1}.) [For reference, for a nominally similar bundle configuration, Nohtomi *et al.* reported an approximate counting efficiency of $\sim$ 1.3 counts s^{-1} per mrem hr^{-1} (0.13 counts s^{-1} per μSv hr^{-1}) when measuring the radiation field on the access deck of the YAYOI research reactor [25]. The maximum efficiency for BCF-12 is 10.6 counts s^{-1} per mrem hr^{-1} (1.06 counts s^{-1} per μSv hr^{-1}.) The maximum efficiency for BCF-20 is 13.9 counts s^{-1} per mrem hr^{-1} (1.39 counts s^{-1} per μSv hr^{-1}.) The relative efficiency of each SFB is also presented in Fig. 7. The trend of efficiency versus position along the SFB is consistent among all three sensors. It is worth noting here that the absolute efficiency positively correlates with the number of fibers in the SFB,

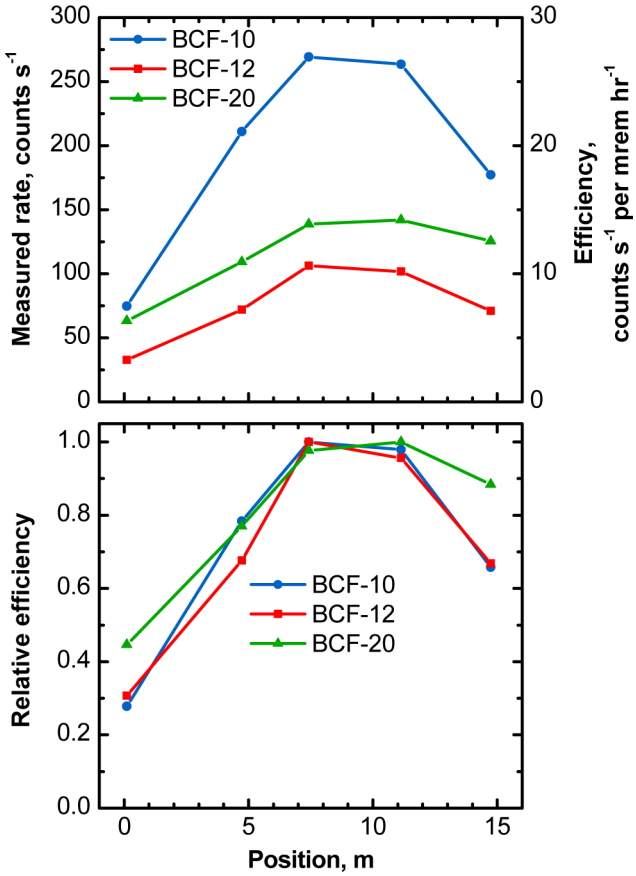

Fig. 7. The top plot shows the measured count rate, and the computed efficiency, for the three SFBs measuring a 10 mrem hr^{-1} ^{137}Cs source. The lower plot shows the position-dependent relative efficiency, with each SFB normalized to its maximum count rate.

considerably more fibers could be included in a single SFB. However, this scaling may not be linear. It is possible that the total SFB efficiency may be more than the sum of the efficiency per fiber as Compton-scattered electrons generated in one fiber (leading to a scintillation in that fiber) have a chance to interact in nearby fibers as well. This relationship awaits further study.

With regard to detection efficiency it should be noted that the Hamamatsu R9800 PMTs used for this project are not nearly as well suited for BCF-20 as they are for BCF-10 and BCF-12, as illustrated in Fig. 2. Because of the lower quantum efficiency of the R9800 tubes at the peak emission wavelength of BCF-20 it was more difficult to discriminate signal pulses from noise events, leading to a degraded pulse triggering and detection probability in the data acquisition system. A higher-efficiency PMT, such as the R7600U-20-M4 photomultiplier by Hamamatsu, would be worth considering for applications requiring much longer sensors, where the improved 1/e-length of BCF-20 would become a dominant factor in fiber selection. The choice to use the same PMT and data acquisition equipment was made primarily to facilitate head-to-head comparisons for position linearity and resolution.

E. Linearity Versus Rate

A separate test was performed to examine the linearity in response for BCF-10 versus dose rate. This test used a partially

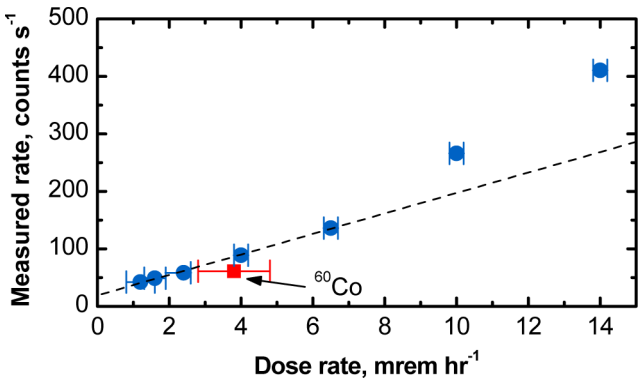

Fig. 8. Test of the linearity of the BCF-10 SFB, measured at the center of the SFB, for varying ^{137}Cs dose rates from 1.2 mrem hr^{-1} to 14 mrem hr^{-1}. Also shown here is the BCF-10 SFB response to a 3.8 mrem hr^{-1} ^{60}Co source.

collimated ^{137}Cs check source. The test started by resting the center of the SFB against the check source to achieve the maximum dose rate, 14 mrem hr^{-1} (1.4 mSv hr^{-1}.; note: does rates for these measurements, as well as for other measurements in this paper, were measured using a calibrated laboratory health-physics instrument.) Tungsten plates were then placed around the check source to separate the distance between the source and SFB—decreasing the dose rate at the SFB. The maximum stand-off depth for the check source from the SFB was 6.7 cm, producing a dose rate of 1.2 mrem hr^{-1} (0.12 mSv hr^{-1}.) Measurements were made at seven different positions; the results are shown in Fig. 8. An acceptable $(R^2 = 0.9965)$ linear fit has been applied to the < 7 mrem hr^{-1} data in the plot. However, it appears that for the bare case and for the case with minimal collimation (7 mm, 10 mrem hr^{-1} (0.10 mSv hr^{-1}) a greater section of the SFB was exposed to the source (the two right-most data points in Fig. 8.) (This collimation approach was not effective in exposing a uniform section of SFB; unfortunately, a variable yield radiation source was not available for these tests.) In this non-ideally collimated case, however, the BCF-10 SFB appears to provide a conservative estimate of dose field in terms of radiological health protection. A measurement made using the ^{60}Co source is also presented on this plot.

V. Summary

SFB linear detector sensors can effectively detect low-level gamma-ray radiation fields over long distances in a continuous fashion. The position response for locating events is linear over a range of 15 m and the sensors exhibit a spatial resolution of 0.5 to 0.6 m, depending upon fiber type and position along the fiber. Their efficiency has been measured to be from 3.3 counts s^{-1} per mrem hr^{-1} to 26.9 counts s^{-1} per mrem hr^{-1} (0.33 counts s^{-1} per μSv hr^{-1} to 2.69 counts s^{-1} per μSv hr^{-1}) depending upon fiber type and location along the SFB. For the PMT and data acquisition set-up used here BCF-10 is the most efficient of the three fiber-types studied, while BCF-12 is the least efficient. This effort has shown that a roughly ~20-fold improvement in detection efficiency can be achieves with BCF-10 when using higher-performing PMTs together with a high-rate digital waveform data acquisition system. This paper has confirmed prior measurements of linearity with BCF-10 SFBs and demonstrated the suitability of this technique with other types of scintillating fiber materials.

With the best spatial resolution as well, BCF-10 appears to be the best candidate fiber, of the three studied, for use in sensor arrays of length ~ 15 m or less. However, with the longest 1/e length, the BCF-20 fiber type may be a better choice for longer length sensors. The relative availability of PMTs matched to the wavelength of BCF-10 also makes it a strong candidate. However, noting that the long-distance detection efficiency and performance from a BCF-20 SFB could likely be improved by choosing a different PMT with a spectral response more closely matched to the longer-wavelength output spectrum of this fiber, a system designed for longer distances might still benefit from BCF-20. Also, even though the R9800 PMTs were used, this effort has shown that BCF-10,12, and 20 demonstrate similar linear performance along 15-m SFBs.

Acknowledgment

The authors would like to thank Dr. Michael Mayhugh of Saint-Gobain Crystals for his assistance preparing the SFB assemblies used in this project and for providing assistance with the concept and testing. They would also like to thank Prof. Akihiro Nohtomi of Kinki University, Japan, for his thoughtful suggestions and guidance early on in this project.

References

[1] G. T. Reynolds and P. E. Condon, "Filament scintillation counter," *Rev. Sci. Inst.*, vol. 28, pp. 1098–1099, 1957.
[2] E. L. Chupp and D. J. Forrest, "A directional neutron detector for space research use," *IEEE Trans. Nucl. Sci.*, vol. NS-13, pp. 468–477, 1966.
[3] M. Atkinson *et al.*, "Initial tests of a high resolution scintillating fibre (SCIFI) tracker," *Nucl. Inst. Meth. Phys. Res. A*, vol. 254, pp. 500–514, 1987.
[4] G. A. Wurden *et al.*, "A Scintillating-Fiber 14-MeV Neutron Detector on TFTR During DT Operation," Report LA-UR-94–1604, Los Alamos National Laboratory, Los Alamos, NM, USA, 1994.
[5] D. Holslin *et al.*, "A directional fast neutron detector using scintillating fibers and an intensified ccd camera system," *Nucl. Inst. Meth. Phys. Res. A*, vol. 353, pp. 118–122, 1994.
[6] W. C. Sailor *et al.*, "Conceptual design for a scintillating-fiber neutron detector for fusion reactor plasma diagnostics," *Rev. Sci. Inst.*, vol. 66, pp. 898–900, 1995.
[7] D. Ress *et al.*, "High-sensitivity scintillating-fiber imaging detector for high-energy neutrons," *Rev. Sci. Inst.*, vol. 66, pp. 4943–4948, 1995.
[8] Q. Zhang, Q. Wang, and Z. Xie, "Detection of fast neutrons using a new scintillating-fiber-array neutron detector," *Nucl. Inst. Meth. Phys. Res. A*, vol. 496, pp. 228–232, 2003.
[9] R. F. Grazioso *et al.*, "Feasibility of using boron-loaded plastic fibers for neutron detection," *Nucl. Inst. Meth. Phys. Res. A*, vol. 422, pp. 59–63, 1999.
[10] M. Yamashita, T. Nozaki, and K. Ninomiya, "Development of a sheet type contamination monitor using the plastic scintillation fiber (PSF)," in *10th Congress Int. Rad. Prot. Assoc.*, Hiroshima, Japan, May 14–19, 2000.
[11] K. H. Abel *et al.*, "Scintillating-glass-fiber neutron sensors," *Nucl. Inst. Meth. Phys. Res. A*, vol. 353, pp. 114–117, 1994.
[12] R. Ruchti *et al.*, "Development of new scintillating fiber detectors for high energy physics applications," *IEEE Trans. Nucl. Sci*, vol. 36, pp. 146–149, 1989.
[13] C. Angelini *et al.*, "High-resolution tracking with scintillating fibers," *Nucl. Inst. Meth. Phys. Res. A*, vol. 277, pp. 132–137, 1989.
[14] C. D'Ambrosio *et al.*, "Particle tracking with scintillating fibers," *IEEE Trans. Nucl. Sci.*, vol. 43, pp. 115–2127, 1996.
[15] E. P. Q. Alcón, R. T. Lopes, and C. E. V. de Almeida, "EPR study of radiation stability of organic plastic scintillator for cardiovascular brachytherapy Sr^{90}-Y^{90} beta dosimetry," *App. Rad. Iso.*, vol. 62, pp. 301–306, 2005.

[16] A. S. Heger *et al.*, "Use of Neutron-Capture Plastic Fibers for Nondestructive Assay," Report LA-UR-98–3054, Los Alamos National Laboratory, Los Alamos, NM, USA, 1998.
[17] W. Koechner, "Radiation sensitive optical fiber and detector," U.S. patent 4,788,436, Nov. 29, 1988.
[18] A. S. Beddar, T. R. Mackie, and F. H. Attix, "Cerenkov light generated in optical fibers and other light pipes irradiated by electron beams," *Phys. Med. Biol.*, vol. 37, pp. 925–935, 1992.
[19] D. Fluhs *et al.*, "Direct reading measurement of absorbed dose with plastic scintillators—the general concept and applications to ophthalmic plaque dosimetry," *Med. Phys.*, vol. 23, pp. 427–434, 1996.
[20] A. S. Beddar *et al.*, "A miniature "Scintillator-fiberoptic-PMT detector system for the dosimetry of small fields in stereotactic radiosurgery," *IEEE Trans. Nucl. Sci.*, vol. 48, pp. 924–928, 2001.
[21] S.-I. Imai *et al.*, "New radiation detector of plastic scintillating fiber," *Rev. Sci. Inst.*, vol. 62, pp. 1093–1097, 1991.
[22] E. Takada *et al.*, "Neutron radiation distribution sensor using flexible plastic scintillating fiber combined with the time-of-flight technique," *IEEE Trans. Nucl . Sci.*, vol. 42, pp. 570–574, 1995.
[23] T. Oka *et al.*, "Development of fiber optic radiation monitor using plastic scintillation fibers," *J. Nucl. Sci. Tech.*, vol. 35, pp. 857–864, 1998.
[24] D. Makowski *et al.*, "A distributed system for radiation monitoring at linear accelerators," *IEEE Trans. Nucl. Sci.*, vol. 53, pp. 2008–2015, 2006.
[25] A. Nohtomi *et al.*, "On-line evaluation of spatial dose-distribution by using a 15m-long plastic scintillation-fiber detector," in *IEEE Nucl. Sci. Symp. Conf. Rec.*, 2008, pp. 965–968.
[26] Scintillating Products, Scintillating Optical Fibers, Product Brochure, Saint Gobain Crystals, Hiram, OH, USA [Online]. Available: www.detectors.saint-gobain.com
[27] Photomultiplier tube R9800, Product Brochure TPMH1298E04, Hamamatsu Photonics, Iwata City, Japan, 2010.
[28] P. Zugec, "A timing resolution model for scintillating fibers," in *IEEE Nucl. Sci. Symp. Conf. Rec.*, 2011, pp. 1605–1608.
[29] P. Zugec, "A timing resolution model for scintillating fibers," in *Nucl. Sci. Symp. Conf. Rec.*, Valencia, Spain, Oct. 23–29, 2011.